DESIGN OF A CIRCULAR REFLECTARRAY WITH A PERFORMANCE COMPARABLE TO THE TYPICAL RECTANGULAR REFLECTARRAY

A Thesis
Presented to
The Academic Faculty

by

Joshua S. Roper

In Partial Fulfillment
of the Requirements for the Degree
Master of Science in the
School of Electrical and Computer Engineering

Georgia Institute of Technology
December 2017

DESIGN OF A CIRCULAR REFLECTARRAY WITH A PERFORMANCE COMPARABLE TO THE TYPICAL RECTANGULAR REFLECTARRAY

Approved by:

Dr. Andrew F. Peterson, Advisor
School of Electrical and Computer Engineering
Georgia Institute of Technology

Dr. Madhavan Swaminathan
School of Electrical and Computer Engineering
Georgia Institute of Technology

Dr. Gregory D. Durgin
School of Electrical and Computer Engineering
Georgia Institute of Technology

Date Approved: December 6th, 2017

TABLE OF CONTENTS

LIST OF FIGURES

SUMMARY

A circular reflectarray is a novel design combining the unit-ring artificial magnetic conductor with the reflectarray concept. It is shown through simulation that a circular reflectarray with either concentric or radial polarization can be designed with basic performance metrics (directivity, sidelobe level and bandwidth) that are comparable or even better than a conventional rectangular design. It is one goal of this work to explore 2D curvature – using the unit-ring approach – in the realm of reflectarrays designed with circular symmetry. Reflectarrays are chosen as the application to explore these issues as the design process used in creating them borrows from reflector antennas, periodic structures and array theory – thus curvature can be explored from a variety of design domains.

Chapter 1

Introduction

One of the most fundamental problems in electromagnetics engineering is to use engineered material to affect electromagnetic radiation before it reaches a receiver. Examples include using a parabolic reflector in conjunction with an antenna to drastically improve antenna gain, using frequency selective surfaces to allow multiple feeds to share a single reflector, using an artificial magnetic conductor to allow for low profile antenna applications, and using multiple periodic radiating elements on a planar surface – called a reflectarray – as an alternative to reflector antennas in order to provide similar performance but on a planar surface with optional adaptive capabilities. This thesis will consider the design of reflectarrays.

Due to system-level considerations, antennas and microwave structures may take a backseat to mechanical structures or other hardware. For example, in aerospace applications, antennas may be placed conformal to curved locations such as the wing of a plane or the nose of a missile to provide a lower profile, mitigate integration costs and lower radome performance needs. In cases such as these, methods of design and analysis for three-dimensional, doubly curved surfaces may be employed [1].

However, given a conformal geometry – especially in regards to periodic structures – complications in design and analysis arise. A typical plane wave will have a phase of:

$$e^{-jkx} = e^{-jka\cos(\theta)} \tag{1}$$

It can be seen that sampling in $\hat{x}$ produces a linear phase shift while sampling in $\hat{\theta}$ produces a non-linear phase shift as seen in figures #1 and #2. This behavior suggests that designing a

curved periodic structure will not yield the same simple Floquet condition of a scalar multiplier as in the rectangular periodic case [2], namely:

$$E_z^{inc}(x+ma, y+nb) = E_z^{inc}(x,y)e^{-jk_x^{inc}ma}e^{-jk_y^{inc}nb} \quad (2)$$

Thus, when designing curved periodic structures, the Floquet condition in its conventional form may not be applied due to the non-linearity of the response. It is one goal of this work to explore 2D curvature – using the unit-ring approach [3] – in the realm of reflectarrays designed with circular symmetry. Reflectarrays are chosen as the application to explore these issues as the design process used in creating them borrows from reflector antennas, periodic structures and array theory – thus curvature can be explored from a variety of design domains [4]. A long term goal is that some of the ideas and methods could be applied in the future to more complex antennas and periodic structure geometries exhibiting 3D curvature.

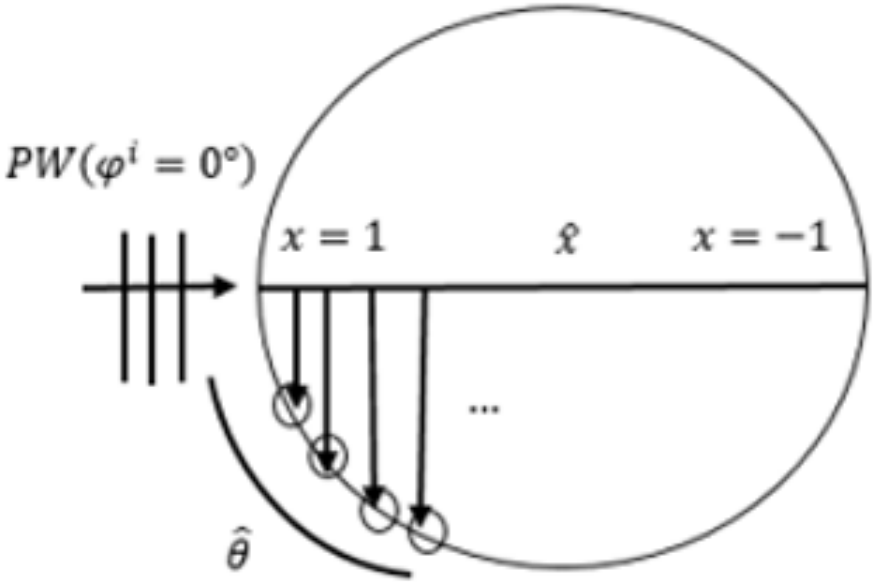

Fig. 1 – Sampling Schemes of a Plane Wave

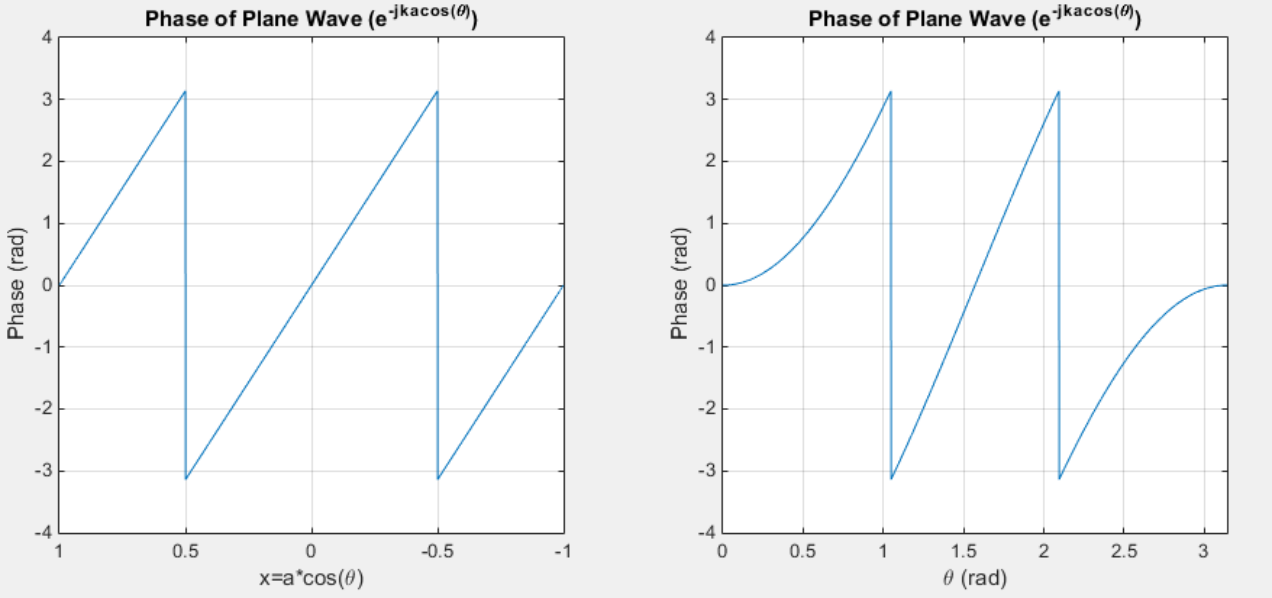

Fig. 2 – (a) Cartesian Phase Sampling (b) Polar Phase Sampling

Chapter 2

Literature Review

Section #2.1: Review of Reflector Theory and Literature

The oldest form of electromagnetic radiation shaping is the reflector: the original form of which is the simple optical mirror (plane reflector) and traces its origins into prehistory. The first microwave frequency reflector antenna was designed by Hertz in 1888 using a cylindrical parabolic reflector. Geometric optics predicts that any coherent radiation incident on a parabolic reflector will come to some focal point "F". In a single reflector system, an antenna or "feed" is placed at the focal point in order to absorb all of the electromagnetic energy ejected from the reflector [5].

Dual reflector antennas are based upon the early optical telescope designs of Gregory (1663) and Cassegrain (1672) and include a subreflector for the feed to illuminate, rather than illuminate the main reflector directly. The two main configurations are the "Cassegrain" with a hyperbolic convex subreflector located before the virtual focal point and the "Gregorian" with an elliptical concave subreflector located beyond the virtual focal point. Both types can be seen in figure #3. Dual reflector antennas allow for much lower noise applications due to the feed location in the apex of the main reflector rather than at the feed point "F". This eliminates the need for a large portion of transmission lines, thereby eliminating transmission line losses. Also, the radiation spillover from the subreflector is now being directed toward the low temperature sky, rather than the high temperature ground [6].

The parabolic reflector can be designed using simple equations and principles. The following equations, with the terms defined by the pictures below present a method of design:

$$\rho' = 2F\tan\left(\frac{\theta_f}{2}\right) \rightarrow Reflector\ Geometry \tag{3}$$

$$\theta_0 = 2\tan^{-1}\left(\frac{1}{4\left(\frac{F}{D}\right)}\right) \rightarrow Feed\ 10dB\ Half\ Beamwidth \tag{4}$$

$$E_{Aperture\ Illumination}(\rho') = F_{Feed\ Patern}\left(\theta_f = 2\tan^{-1}\left(\frac{\rho'}{2F}\right)\right)\frac{1}{1+\left(\frac{\rho'}{2F}\right)^2} \tag{5}$$

$$Edge\ Illumination = 20\log\left[E_{Ap.Illum.}(\rho' = a)\right] = -Edge\ Taper \tag{6}$$

$$Feed\ Taper = F_{Feed\ Patern}(\theta_0) \tag{7}$$

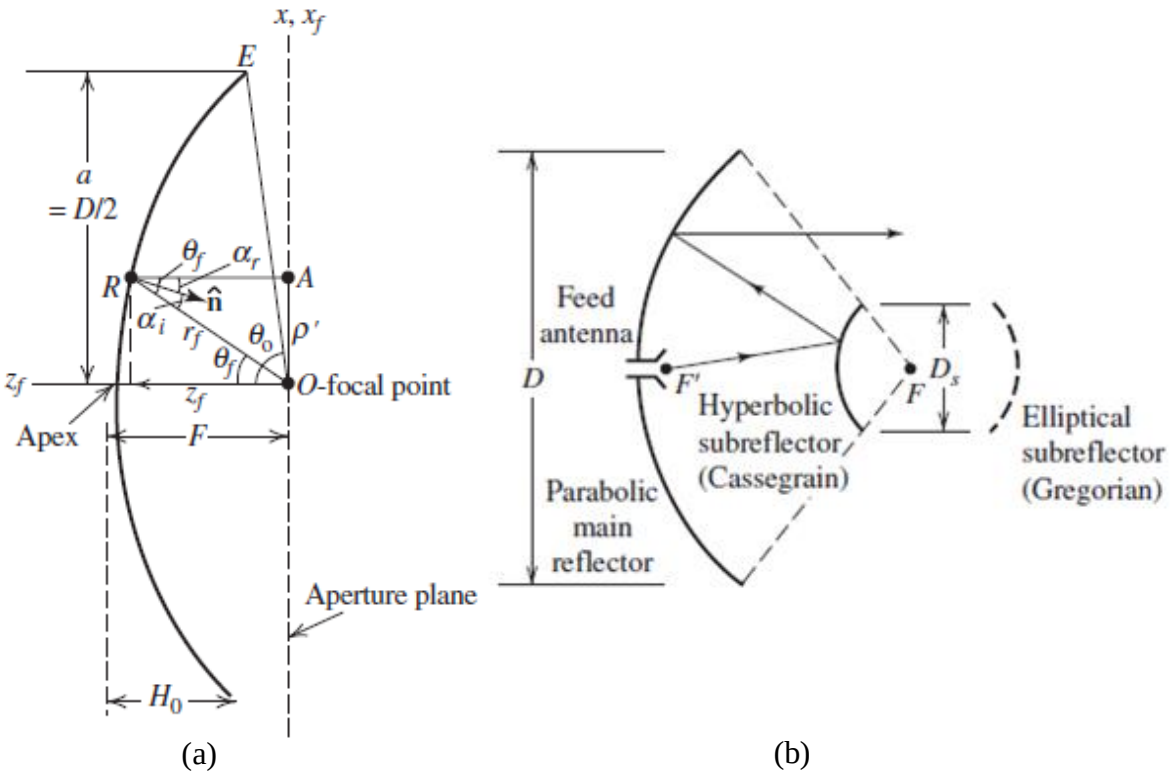

Fig. 3 – (a) Parabolic Reflector Cross-Section [5] (b) Dual-Reflector Antennas [5]

Section #2.2: Review of Periodic Structures – AMCS and FSSs

One fundamental concept of reflective surface engineering is that of the frequency selective surface (FSS). An FSS is a periodic microwave structure that acts as a frequency specific filter: specifically, it acts as a bandpass filter for a certain frequency range, and it acts as a bandstop filter for all other frequencies [7].

In dual-reflector systems, an FSS can be applied to the subreflector to allow for multiple non-collocating feeds to share the same main reflector or to improve performance – see figure #4 [8-9]. Consider the following real world application: a multifrequency dual-reflector system operating at both X-band (8-12 GHz) and S-band (2-4 GHz) frequencies. In the figure below, the S-band would be feed f2, and the FSS subreflector would act as a passband filter to allow the radiation to pass through the FSS subreflector. Meanwhile, feed f1 would see the FSS as a stopband filter and operate as an offset feeds interacting with a solid conducting surface [8-9].

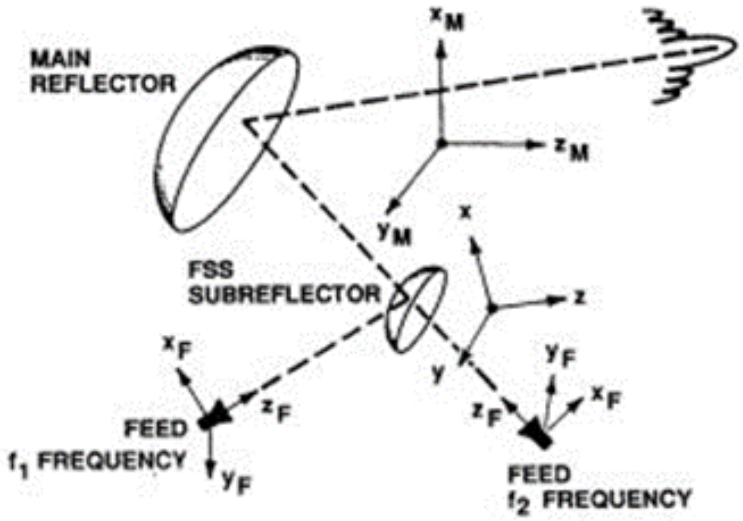

Fig. 4 – Collocating Feeds Using a FSS [8]

Another periodic microwave structure that is used to alter the reflection of electromagnetic waves is the artificial magnetic conductor (AMC). The AMC is a uniform periodic tiling of microstrip elements designed to give a uniform phase front with a certain phase shift – specifically 90º. An AMC is a type of high-impedance surface (HIS) that exhibits an electromagnetic band-gap (EBG) which prohibits surface wave propagation and also exhibits in-phase reflection of incident waves [10].

AMCs can be used to approximate a perfect magnetic conductor (PMC) for a certain narrow bandwidth. An AMC can also be thought of as a single FSS over a dielectric and backed by a perfect electric conductor (PEC). These AMCs are realized using periodic microwave structures, such as a repeating set of microstrip designs or metal corrugations. AMCs are often used as ground planes and omnidirectional antennas are placed flush to the surface. These structures also face a limited bandwidth due to the elements and spatial phase delay.

Normally, omnidirectional radiating structures placed above a copper ground plane must have a $\lambda/4$ spacing in order to not experience destructive interference due to the 90º phase shift of PECs. With an AMC ground plane, it is possible to place the radiating structure immediately on top of the AMC surface. These properties allow for an omnidirectional antenna to be placed flush to the surface on the AMC and experience constructive interference of the backwards reflected waves thus increasing gain and improving radiation efficiency – see figure #5 [11].

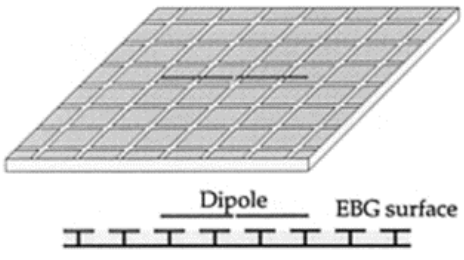

Fig. 5 – AMC Backed Dipole [11]

In order to simulate these periodic structures, an infinite extent approximation is used. In the planar rectangular case, Floquet conditions can be applied to account for the linear phase shifting along the elements in an infinite environment [2]. This allows one to work with a single unit cell rather than the entire surface. Because of this periodicity, an H-wall waveguide simulator can be used for the unit cell (E=0 and H=0 boundary conditions) to simulate an infinite method of images environment [4]. Additional considerations may also be taken into account depending on the type of numerical formulation that is employeed [12], [13]. In this way, mutual coupling effects are taken into account and the amplitude and phase charaterisitcs of the periodic stucture can be found as a function of frequency.

To simulate a curved periodic microwave surface, one of several approximate methods are typically used. A locally planar unit-cell analysis can be conducted to get the reflectance and transmittance parameters and then these can be placed on the surface of a reflector for a diffraction analysis [8]. The square geometry of a patch can be warped into a quasi-trapezoidal shape and analyzed [14-15]. Planar results can be simulated for a rectangular patch and then rotated tangentially around a curved surface using the characteristic basis method and spectral rotation approach [16-17]. However, in order to create a true curved analysis method while still utilizing a unit-cell approach, new symmetry conditions must be taken advantage of and non-rectangular unit-cell grids must be used. For example, cylindrical arrays can be simulated taking advantage of two symmetry planes as in [18]. Another example is simulating a circular AMC by taking advantage of circular symmetry as in [3] and then applied as in [19].

In this work, the approach of [3,19] is taken with regard to simulating the circular periodic structure. In this approach, an FEM solver such as HFSS is used to place the AMC into a cylindrical coax waveguide (see figure #6b) [3,19]. A TEM mode wave is launched down the

waveguide from the feed port and is reflected off of the structure. This experiment is repeated with a PEC slab. The phase or argument of the S11 TEM modes are then taken and the AMC phase is subtracted from the PEC phase to obtain the reflection phase profile of the structure. A comparison of the Cartesian unit-cell and the Unit-Ring are found in figure #6 and a reflection phase profile example is found in figure #7. An AMC with a phase shift in-between -90 and 90 degrees is considered to approximate a perfect magnetic conductor (PMC).

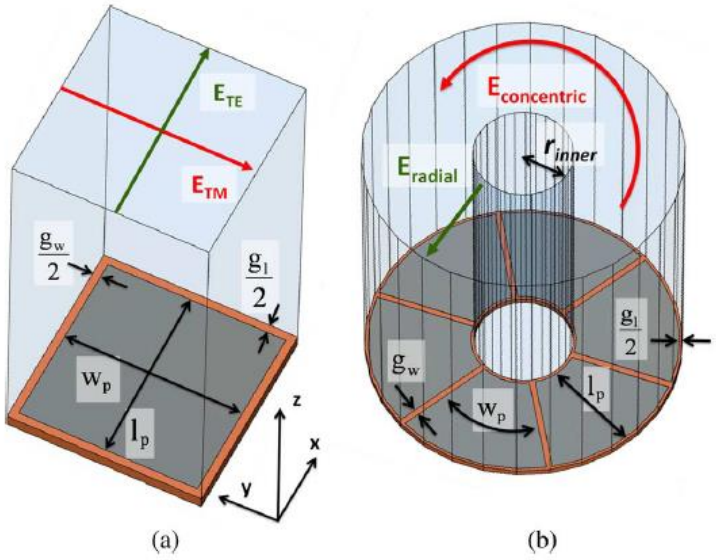

Fig. 6 – (a) Cartesian Unit-Cell [3] (b) Unit-Ring [3]

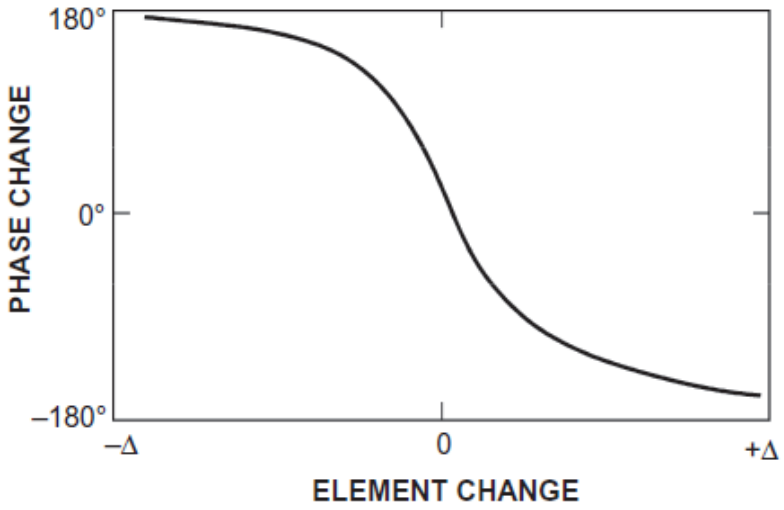

Fig. 7 – Reflection Phase Profile Curve [4]

When simulating the ring geometry in the coaxial environment two dominant types of polarization should be considered: radial and circular. When PEC boundary conditions are applied to the outer and inner conductor walls, then the radial type polarization is produced (fig. 8 (a)). When PMC boundary conditions are applied to the outer and inner conductor walls, then the circular type polarization is produced (fig. 8 (b)). For the purposes of reflectarray simulation, the circular polarization is used to simulate a circularly polarized horn antenna feed.

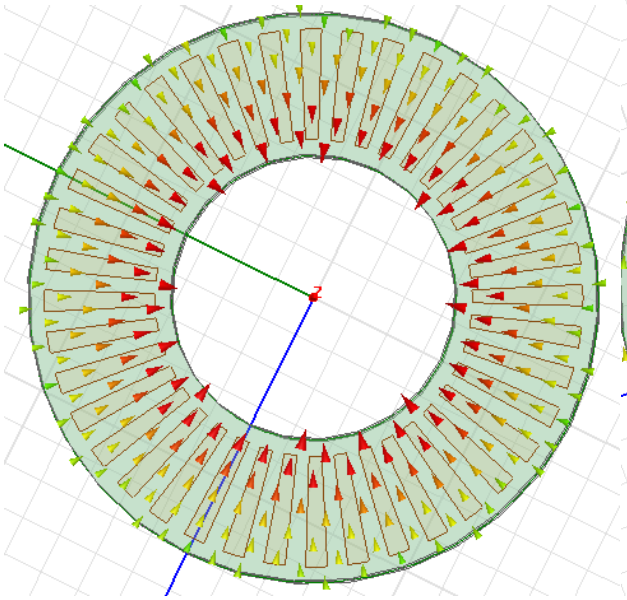

Fig. 8(a) PEC Boundaries to Produce Radial Polarization

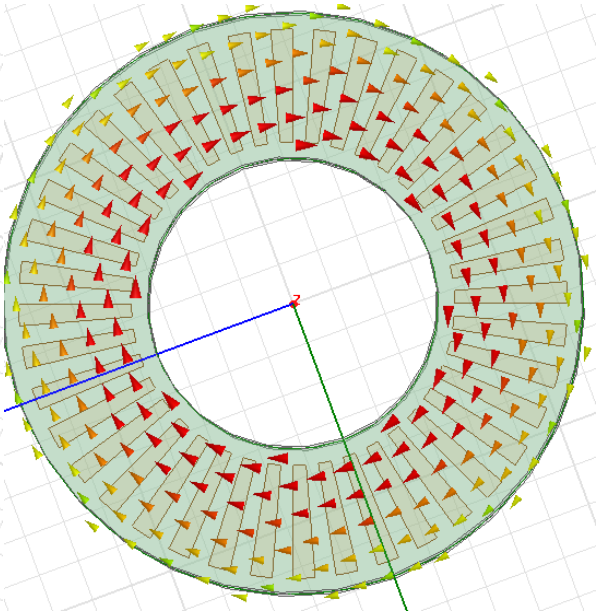

Fig. 8(b) PMC Boundaries to Produce Concentric/Circular Polarization

Section #2.3: Review of Reflectarray Theory and Literature

An antenna concept that combines design and analysis techniques from the reflector antenna, periodic microwave structures (FSS/AMC) and antenna array theory is the reflectarray – which has been around from at least the 1960s [20]. At that time research was focused on waveguide elements. Planar elements such as spirals, discs, and patchs were later explored in the 1970s [21-23]. The first reflectarray patent was filed in the 1980s [24]. This early research was mainly conducted by private companies and the U.S. Air Force for military applications.

It wasn't until the 1990s, that academic research into reflectarray antennas really picked up. Microstrip reflectarray design and theory was fleshed out: particularly analyzing the phase behavior as a function of of patch size through full wave analysis [25-28]. Essential reflectarray capacities were also investigated including: beamsteering [29], multiple polarizations [30], bandwidth improvement [31], and dual-frequencies [32]. Recent advancements have been focused on improving upon these capabilities and enhancing performance metrics.

The reflectarray is a flat surface upon which lie many elements (usually microstrip patches) and where the elements are not connected with power division lines – the general geometry of the reflectarray can be seen in figure #7. This antenna has the benefit of being high gain and good efficiency like the reflector antenna or antenna array, while being flat (unlike the reflector) and not having an expensive, high-loss beamformer (unlike the antenna array). Additionally, low-loss phase shifters can be incorporated to add an electronic beam steering capability (like the antenna array) [33-34]. The reflectarray can also be used as a subreflector, instead of a solid subreflector as reported in [35].

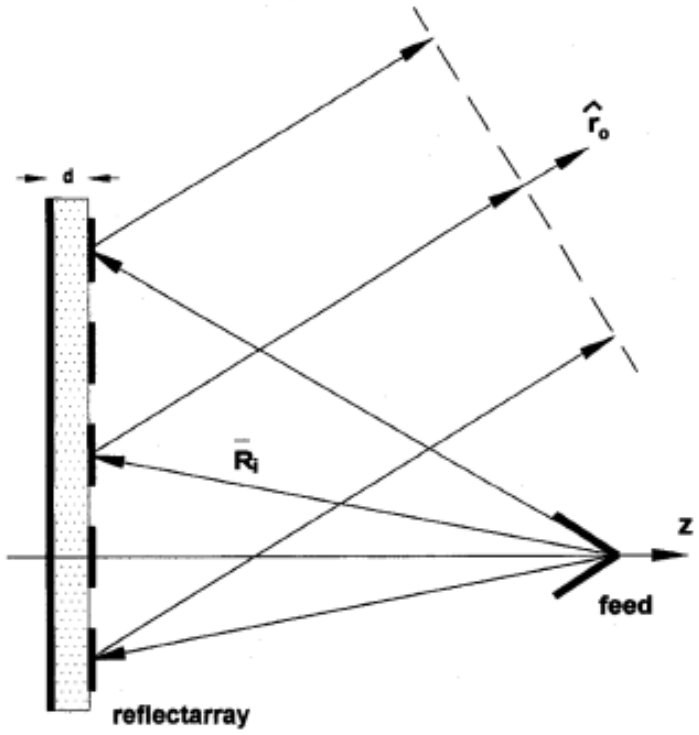

Fig. 9 – Reflectarray Geometry [36]

In contrast to the AMC, the reflectarray will usually have non-uniformly sized elements to produce a non-constant reflected phase. This is from the simple concept that a nearfield source will not produce a uniform wave front, but the desired output of the reflectarray should be a collimated beam – like the reflector antenna. At a basic level, the design must require that a phase shift ψ_i at an element be such the phase delay is constant for all elements. This looks like the following [36]:

$$\mathrm{k}_0(R_i - \bar{r}_i \cdot \hat{r}_o) - \psi_i = 2\pi N \tag{8}$$

where k_0 is the propagation constant, $R_i, \bar{r}_i, and\ \hat{r}_o$ are defined as in figure #9, and N is an integer. Plotting the phase delay or phase shift will generate a series of peaks and nulls around the center of the reflectarray (for a normal angle of incidence). The phase delay curve will look similar to figure #10.

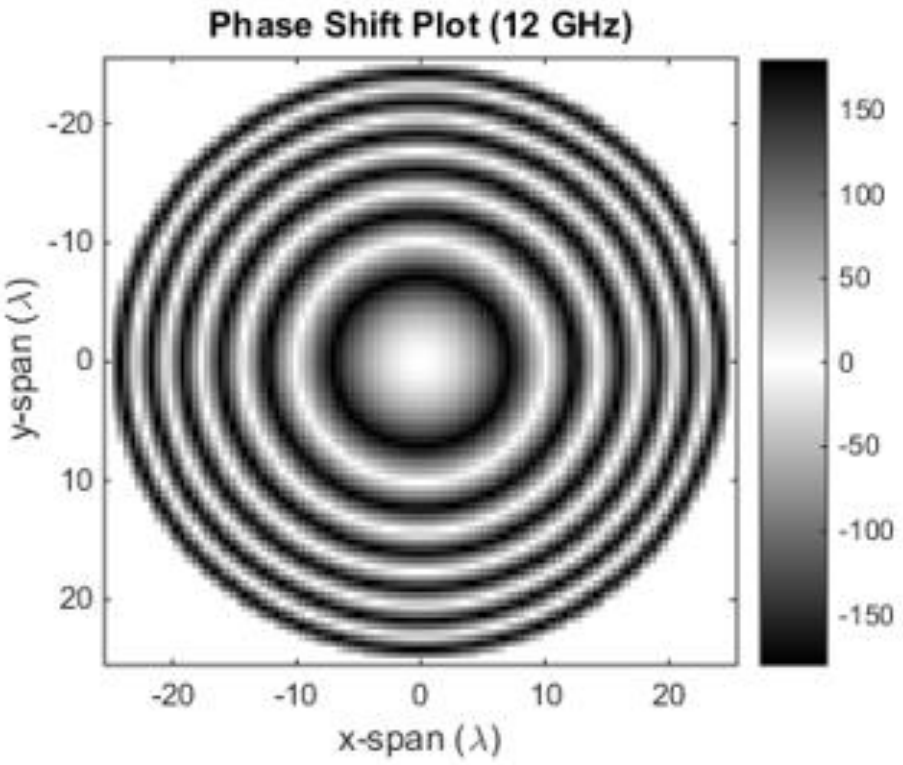

Fig. 10 – Phase Delay Plot

One way to produce the phase delay that is needed for figure 10 is to alter the element size as a function of distance from the center of the array [4]. To design a reflectarray of this type, a full wave simulation of many sized elements will be conducted and then the resulting resonant frequencies will be mapped into a backwards-S curve as depicted in figure 11 below. Then this curve will be used to fit the required phase delay for the reflectarray as depicted in figure 12 below.

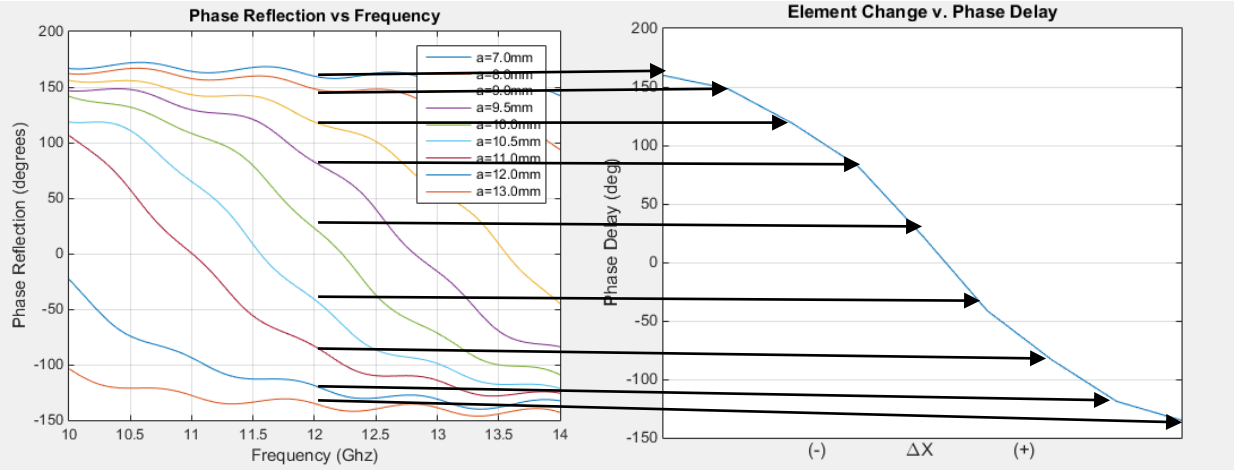

Fig. 11 – Mapping reflection phase vs. frequency to reflection phase vs element size change

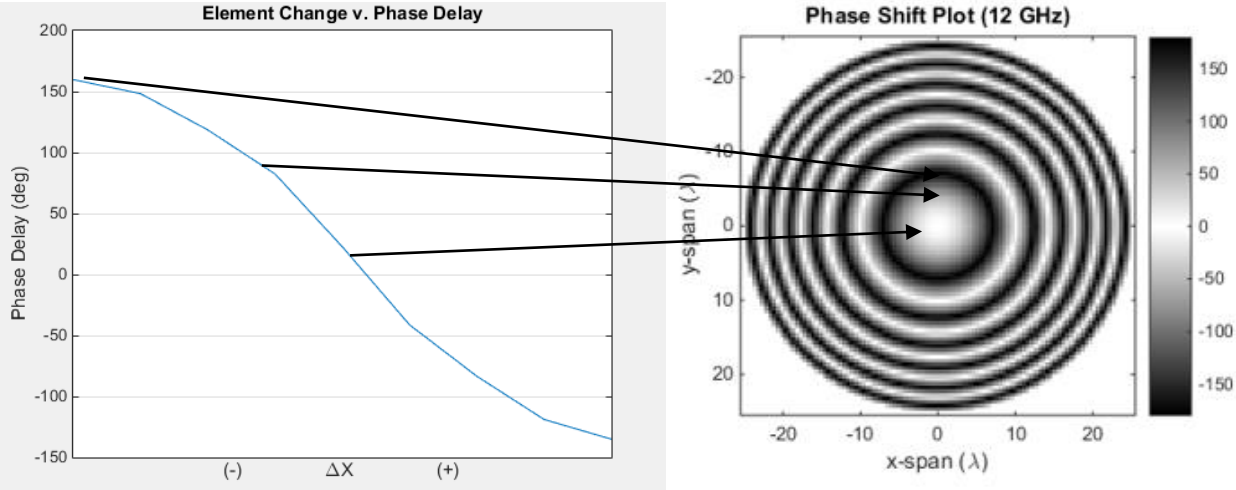

Fig. 12 – Mapping element phase delay to fit the reflectarray required phase delay

Another method of producing a phase delay is to use a transmission line stub, either directly attached to the patch element or coupled through an aperture coupled in the ground plane (see figure 13) [4]. In the case of the attached stub, the stub acts as a transmission line in which the signal enters and is reflected from the end with a certain delay – causing the phase shift of approximately $2\beta\Delta l$. For the coupled stub, a full wave analysis must be performed to find the added delay but it should also be roughly proportional to $2\beta\Delta l$. The coupled stub has a few

benefits over its counterpart: namely, it eliminates spurious reflections by the stubs, allows more room to add a larger delay, and permits active elements such as phase-shifters to be added for adaptive capabilities.

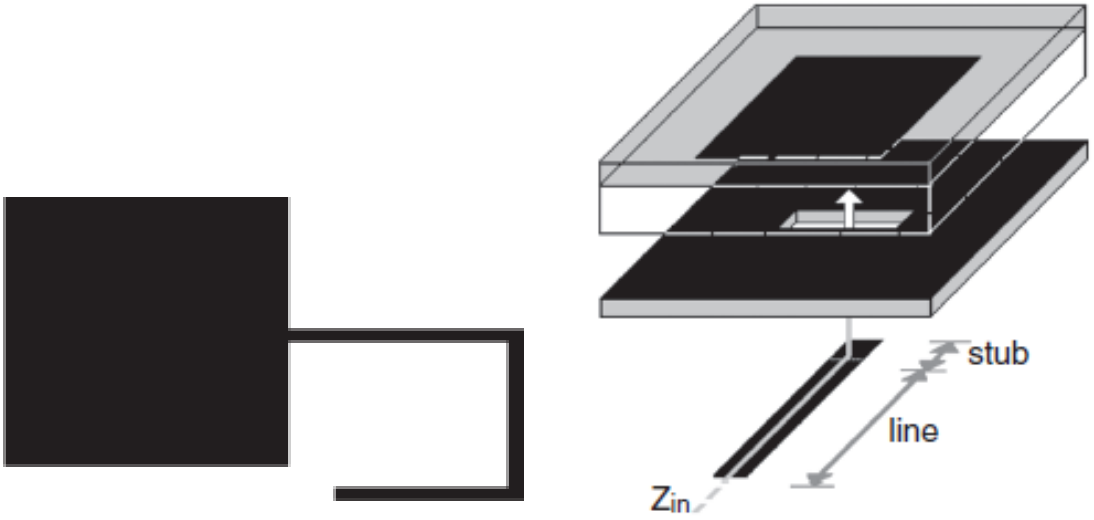

Fig. 13 (a) – Stub Attached to Patch Element [4] (b) Stub Coupled to Patch Through Aperture [4]

The most important characteristic of using these stubs instead of varying the patch size is that the phase change is generated by a true-time-delay [37-38]. This will improve the bandwidth of the reflectarray and remove that limiting factor – leaving only the constrained bandwidth of the radiating element itself. Rather than use the phase delay plot as displayed in figure 12, a true-time-delay plot would look like the following (figure 14):

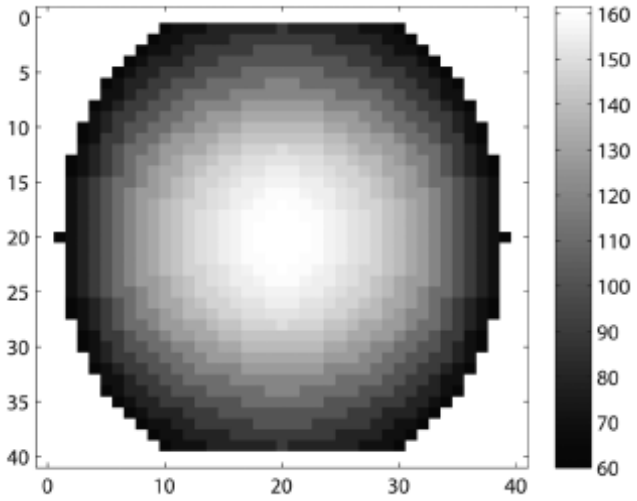

Fig. 14 – A Time-Delay Profile for the Reflectarray (picoseconds) [38]

One of the chief disadvantages of a reflectarray is its lack of bandwidth [4]. This bandwidth limitation is due to both the element selection and the differential spatial phase delay. The most common radiating element used is the microstrip patch, which has a bandwidth of only about 3-5% and limits the entire reflectarray's bandwidth. The differential spatial phase delay is due to the frequency excursion error accumulated as the wave has to necessarily travel a longer distance off of the beam boresight. However, we see that many of these bandwidth issues can be mitigated by using the true-time-delay method of element design.

One final consideration to take into account is dual-band capabilities [4]. In order to work properly over multiple frequency bands, a single unit cell must contain multiple element sizes in that cell. These elements must have small widths (linear or crossed dipoles, circular or square loops, etc.) so that each cell will resonant at two bands. For dual-band applications with close frequencies (say a Tx and Rx band) then the same elements with size diversity will be used (see figure 15a). For dual-band applications with far away frequencies (say Ka-band vs X-band) then different element geometries can be used (see figure 15b).

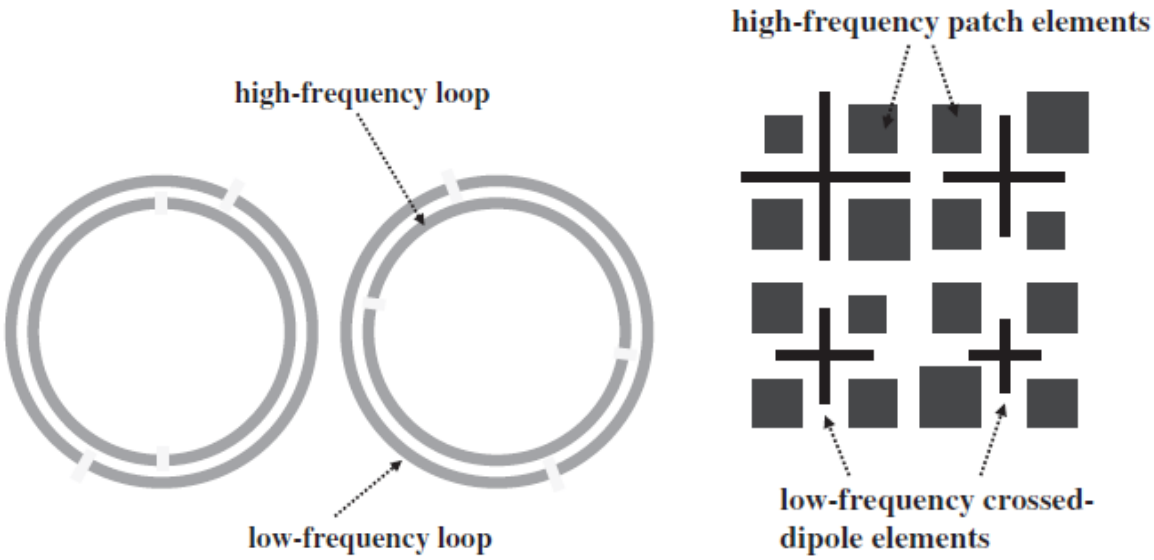

Figure 15 – (a) Closely spaced frequencies [4] (b) Frequencies with large separation [4]

Now that the aperture phase or time distribution has been found as outlined above, the next step in the reflectarray design process is to design the feed. The first part of this process entails choosing an appropriate focal length over reflectarray diameter ratio (F/D ratio), for this example an F/D=1 was chosen. From this the 3dB beamwidth of the feed can be derived from the following equations [4]:

$$\theta_e = \tan^{-1}\left(\frac{1}{2F/D}\right) \rightarrow u = \cos(\theta_e) \tag{9}$$

$$\eta_{spillover} = 1 - u^{2(q+1)} \tag{10}$$

$$\eta_{illumination} = \frac{4(q+1)(1-u^q)^2}{q^2 \eta_{spillover} \tan(\theta_e)^2} \tag{11}$$

$$\eta_{total} = \eta_{spillover}\eta_{illumination} \tag{12}$$

$$q_{max} = \max(\eta_{total}) \tag{13}$$

$$\Rightarrow \boxed{BW_{3dB}(Feed) = 2\cos^{-1}\left(\exp\left\{\frac{\log\left(\frac{1}{2}\right)}{2q_{max}}\right\}\right)} \quad (14)$$

$$BW_{3dB}(Feed) \approx 30° \left(for \frac{F}{D} = 1\right) \quad (15)$$

We see that since we chose a F/D ratio to be 1, then the most efficient beamwidth of our feed is 30 degrees, which lines up with many commercial horn antenna products. An example of the efficiency plots can be seen in figure 16.

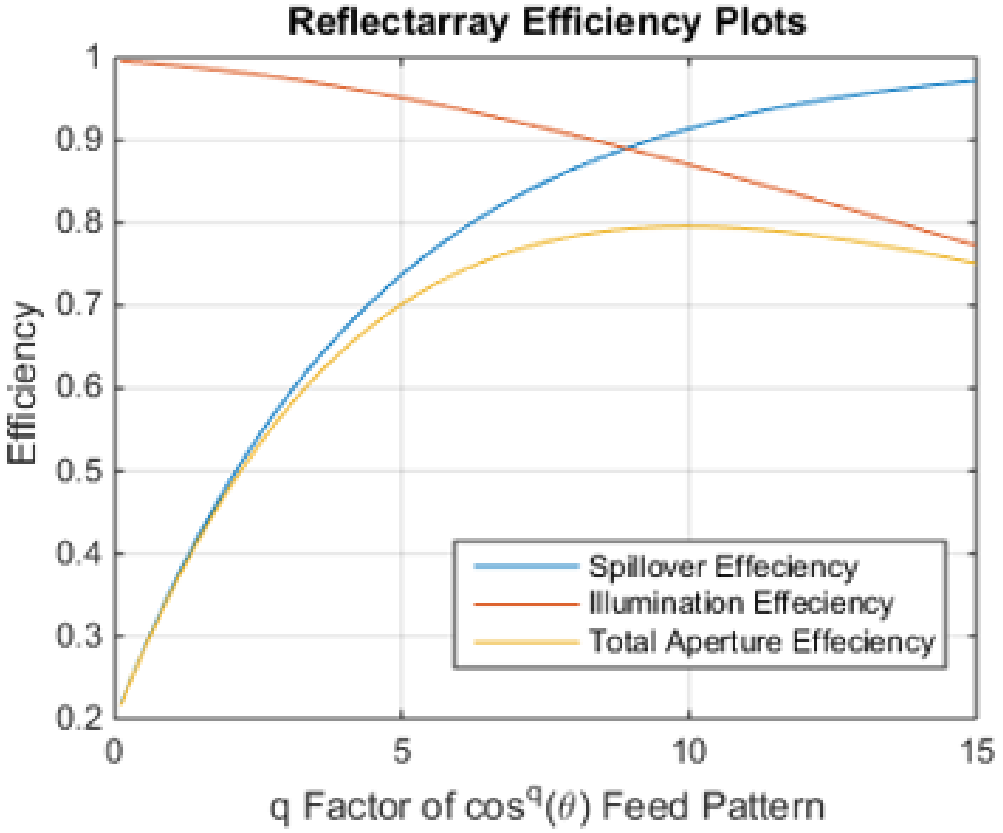

Fig. 16 – Efficiency Plots for Reflectarray to Find Q

Now that the elements and feed have been characterized, the far field can be computed analytically. First we determine the field incident on the reflectarray elements by the following equations [4]:

$$E^{F_X}(\theta,\varphi) = \frac{jke^{-jkr}}{2\pi r}\left[\hat{\theta}\cos^{q_E}(\theta)\cos\varphi - \hat{\varphi}\cos^{q_H}(\theta)\sin\varphi\right] \tag{16}$$

$$E^{F_Y}(\theta,\varphi) = \frac{jke^{-jkr}}{2\pi r}\left[\hat{\theta}\cos^{q_E}(\theta)\sin\varphi + \hat{\varphi}\cos^{q_H}(\theta)\cos\varphi\right] \tag{17}$$

$$\begin{pmatrix} E_X^F \\ E_Y^F \\ E_Z^F \end{pmatrix} = \begin{pmatrix} \sin\theta\cos\varphi & \cos\theta\cos\varphi & -\sin\varphi \\ \sin\theta\sin\varphi & \cos\theta\sin\varphi & \cos\varphi \\ \cos\theta & -\sin\theta & 0 \end{pmatrix}\begin{pmatrix} 0 \\ E_\theta^F \\ E_\varphi^F \end{pmatrix} \tag{18}$$

where "F" notates the feed coordinate system. Now we transform to the reflectarray coordinate system by:

$$\boldsymbol{E}^{RC} = \boldsymbol{A}\boldsymbol{E}^{FC} \tag{19}$$

Now the far field can be solved for by:

$$E(\theta,\varphi) = jk\left[\left(\hat{\theta}\cos\varphi - \hat{\varphi}\sin\varphi\cos\theta\right)\tilde{E}_{R_X}(u,v) + \left(\hat{\theta}\sin\varphi + \hat{\varphi}\cos\varphi\cos\theta\right)\tilde{E}_{R_Y}(u,v)\right]\frac{e^{-jk_0r}}{2\pi r}$$

$$where\ \tilde{E}_{R_i}(u,v) = \iint_{RA} E_{R_i}(x,y)e^{jk_0(ux+vy)}dxdy \tag{20}$$

After some simplifications the radiation pattern can be found to be:

$$E_\theta(\theta,\varphi) = \frac{jke^{-jkr}}{2\pi r}\left(\tilde{E}_{R_X}(u,v)\cos\varphi + \tilde{E}_{R_Y}(u,v)\sin\varphi\right) \tag{21}$$

$$E_\theta(\theta,\varphi) = -\frac{jke^{-jkr}}{2\pi r}\cos\theta\left(\tilde{E}_{R_X}(u,v)\sin\varphi - \tilde{E}_{R_Y}(u,v)\cos\varphi\right) \tag{22}$$

The above analytical model to finding the far field of the reflectarray can be resource intensive and difficult to compute so a simpler array theory approximation can be used instead. The following equation can be used to compute the fields [4]:

$$E(\hat{u}) = \sum_{m=1}^{M}\sum_{n=1}^{N} F\left(\vec{r}_{mn}\cdot\vec{r}_f\right)A(\vec{r}_{mn}\cdot\hat{u}_o)\,A(\hat{u}\cdot\hat{u}_o)\exp\left\{jk\left(\left|\vec{r}_{mn}-\vec{r}_f\right|+\vec{r}_{mn}\cdot\hat{u}\right)+j\alpha_{mn}\right\} \quad (23)$$

Where F is the feed pattern function, A is the reflectarray element pattern function, $\vec{r}_{mn}$ is the position vector of the mn-th element and α_{mn} is the required phase term on the mn-th element, and everything else is defined as in figure 17 below.

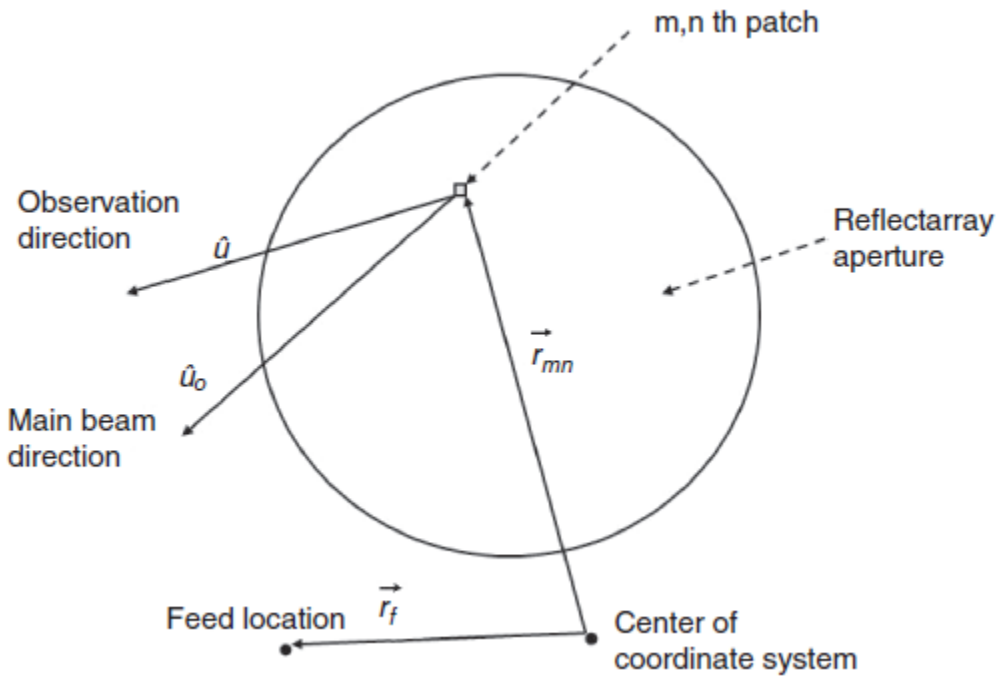

Fig. 17 – The coordinate system of the reflectarray [4]

This formulation can be easily implemented within the MATLAB simulation environment – especially given the sensor array analyzer application in the signal processing toolbox. This has functions to plot the far fields and array geometries based on input.

One array geometry of particular interest is the concentric ring array geometry. This geometry matches with the unit-ring FSS's angular nature and must be employed for this type of periodic structure. This array has the characteristic that in the uniform case relatively high sidelobes occur, to mitigate this, optimal array configurations must be employed. The paper [39] presents techniques to mitigate the sidelobes by as much as 10dB. A serious design would need to employ these techniques as the uniform case would have sidelobe violations for Ku-band as depicted in the following paragraph.

One important consideration for the far field – especially for practical reflectarray designs – are international radiation regulations. The major governing bodies in charge of these include the FCC (USA), ITU (international) and Anatel (Brazil). For the example in this thesis, the FCC regulation for KU-band radiation is considered: CFR § 25.209 Antenna Performance Standards – section "a" subsection "2" as applied to geostationary SATCOM in the ka and ku bands. The figure 18 below depicts the gain envelope given by the regulation. This comes in the form of a pattern mask for which the radiation side lobes must be below – this is to prevent stray radiation from interfering with other communications links.

$29-25\log_{10}\theta$	dBi	For	$1.5° \leq \theta \leq 7°$
8	dBi	For	$7° < \theta \leq 9.2°$
$32-25\log_{10}\theta$	dBi	For	$9.2° < \theta \leq 48°$
−10	dBi	For	$48° < \theta \leq 85°$
0	dBi	For	$85° < \theta \leq 180°$

Fig. 18 – FCC Regulation for ka/ku band communications in geostationary SATCOM

Chapter 3

Design of Planar Reflectarray

In this section, the design process will be reviewed for the conventional reflectarray geometry. A design example using a 25λ diameter reflectarray at 12GHz will be used to provide relevant graphs and illustrations of the design process. Given the 12.5λ radius where each element has a spacing of λ/2, the reflectarray geometry will look as figure 19 below.

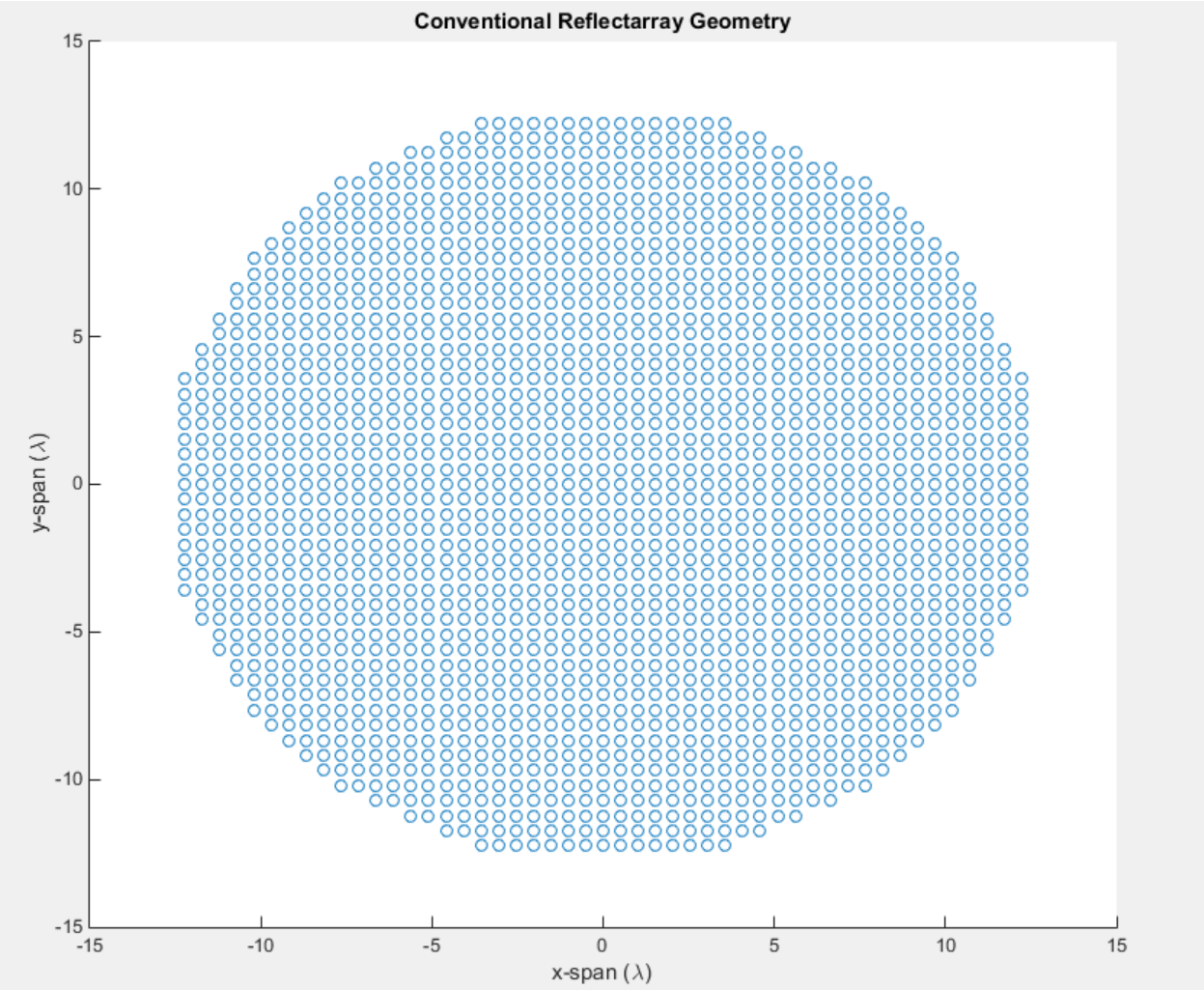

Fig. 19 – Reflectarray Geometry for 25λ Diameter with λ/2 Spacing (1,957 Elements)

Using equation (8), in combination with the geometry of the array and the number of elements, we can generate a phase delay plot. Now that we have this plot we need to perform a full wave simulation to generate phase shift plots as discussed in section 2.2. For this particular planar geometry, HFSS was used to find the phase with each patch being simulated in a waveguide (with a predominately horizontal mode) to approximate infinite extent – with the unit cell size being λ/2. The patch sizes where varied by variable "D" (equal for horizontal and vertical) from -Δ0.5mm to -Δ5.0mm to determine gross phase delay behavior and then by -Δ1.60mm to -Δ2.05mm to determine the phase delay around resonance as defined by the geometry of figure 20 below and the phase curves of figure 21. The bandwidth of this geometry is found to be only about 1.2% for horizontal polarization. As defined by:

$$BW = \frac{f_{-90^o} - f_{+90^o}}{f_{0^o(resonance)}} \tag{24}$$

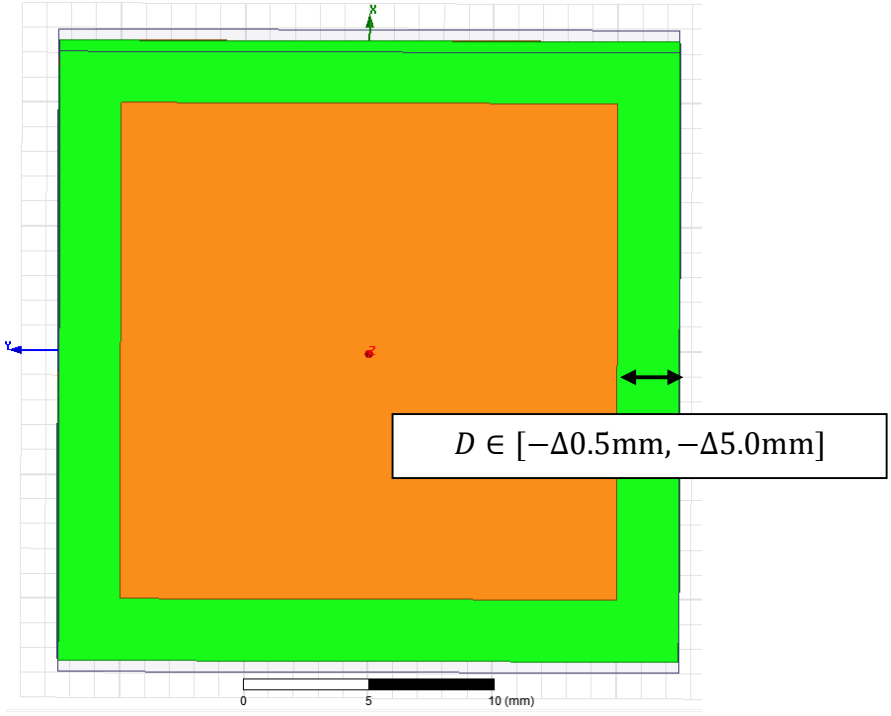

Fig. 20 – Cartesian Patch Element Geometry and Variable "D"

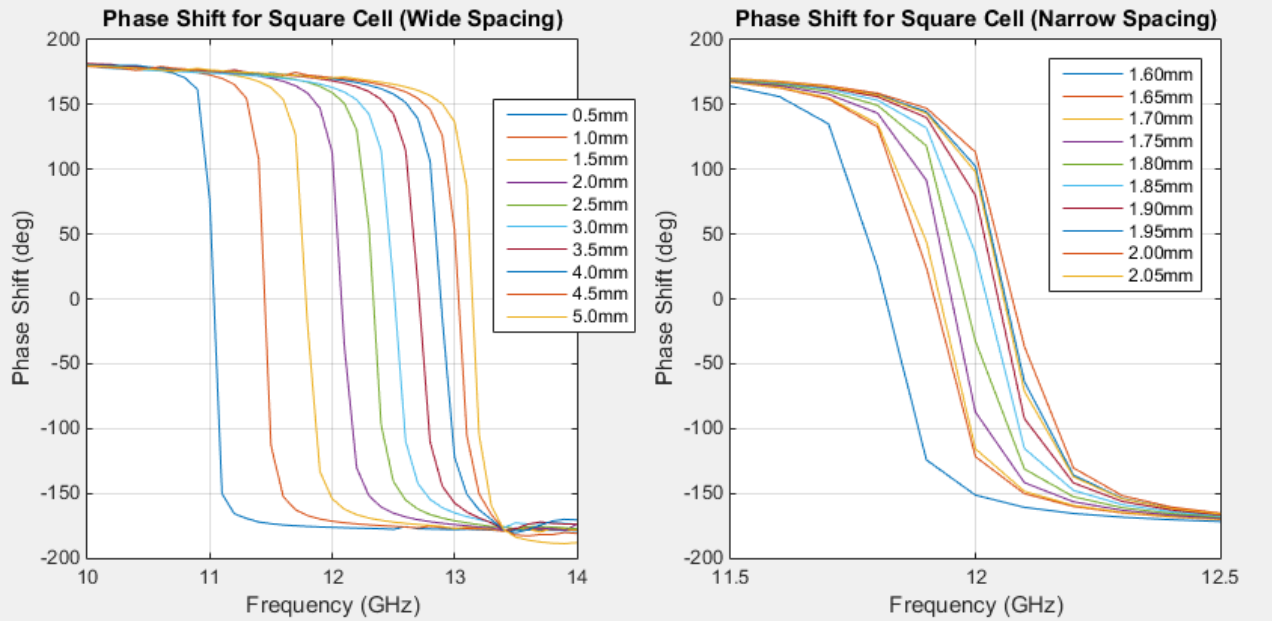

Fig. 21 – Phase Delay Curves Corresponding to Geometry Change "D"

This plot will map element size to a specific phase shift which will be used to map the phase shift on the reflector surface as seen in figure 22.

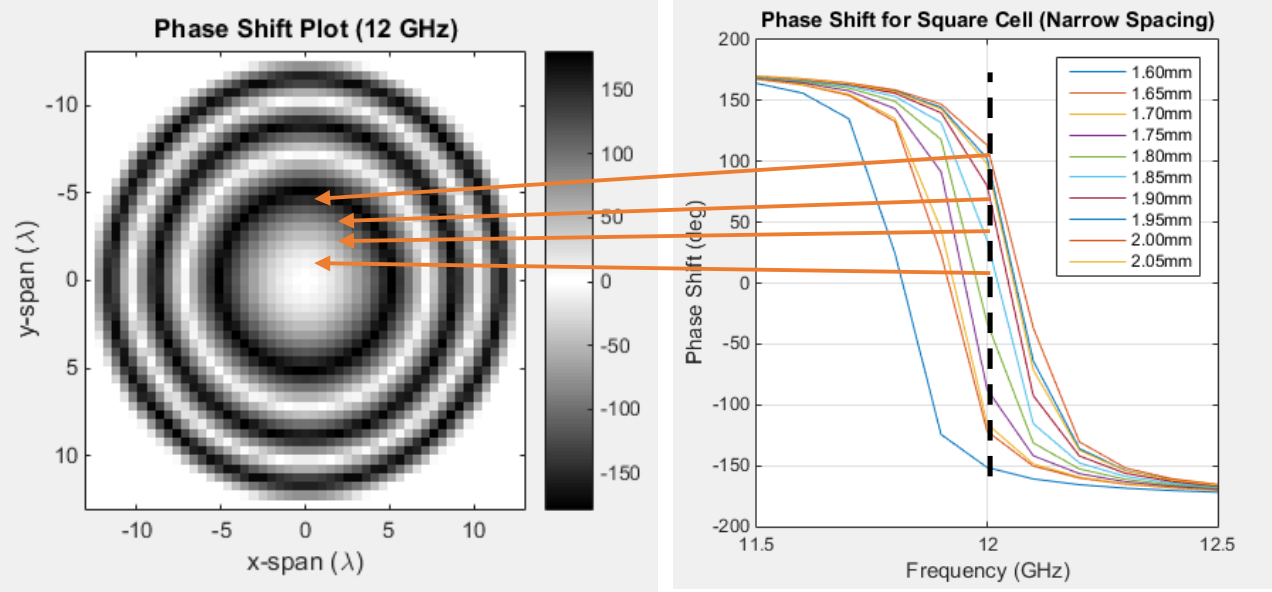

(a) (b)

Fig. 22 – Phase Plot and Matching for 25λ Element Reflectarray

The first part of the design process entails choosing an appropriate focal length over reflectarray diameter ratio (F/D ratio), for this example an F/D=1 was chosen. From this the 3dB beamwidth of the feed can be derived from the following equations: (Eq. (9-15) as above)

$$\theta_e = \tan^{-1}\left(\frac{1}{2F/D}\right) \rightarrow u = \cos(\theta_e)$$

$$\eta_{spillover} = 1 - u^{2(q+1)}$$

$$\eta_{illumination} = \frac{4(q+1)(1-u^q)^2}{q^2 \eta_{spillover} \tan(\theta_e)^2}$$

$$\eta_{total} = \eta_{spillover}\eta_{illumination} \rightarrow q_{max} = \max(\eta_{total})$$

$$\Rightarrow \boxed{BW_{3dB}(Feed) = 2\cos^{-1}\left(\exp\left\{\frac{\log\left(\frac{1}{2}\right)}{2q_{max}}\right\}\right)}$$

Now using our F/D=1, we find that q_{max} is approximately equal to 9.9 – see figure 23.

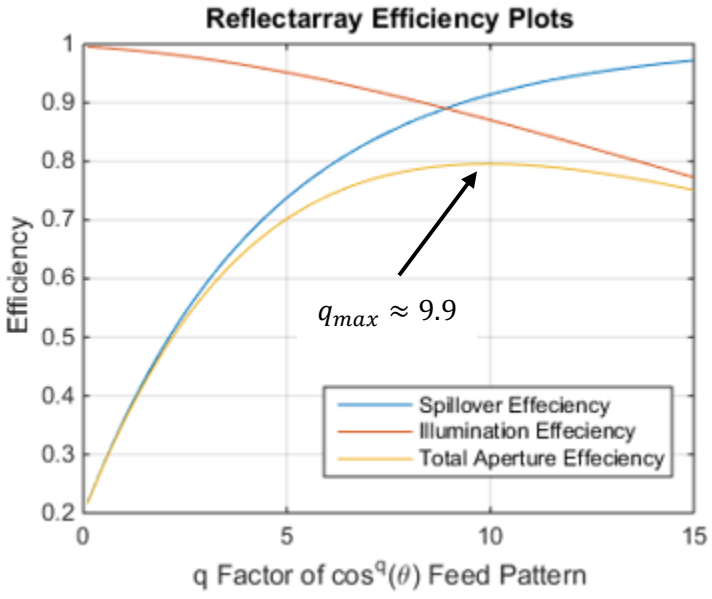

Fig. 23 – Reflector Efficiency Plots

Now using $q_{max} = 9.9$ we can solve for $BW_{3dB}(Feed) \approx 30.14^0$, and we can generate the feed pattern using $\cos^{q_{max}}(\theta)$ as seen in figure 24 (a) while figure 24 (b) just gives the element pattern approximation. Now Figures 24 (a) and (b) are used to find the taper for this reflectarray. Now that we have found everything, we can solve for the far field approximation using MATLAB's "Sensor Array Analyzer" application found in MATLAB's signal processing toolbox by plugging in all the information that we have found.

The far field approximation is seen in figure 25. It has a peak directivity of 37.91dB, with 1.96dB worth of sidelobe margin. This design has a bandwidth of about 1.2%. The feed is located concentric with the center of the array for the pattern that follows (straight vertically up from the center of the array) with a focal length to diameter (F/D) ratio of 1:1.

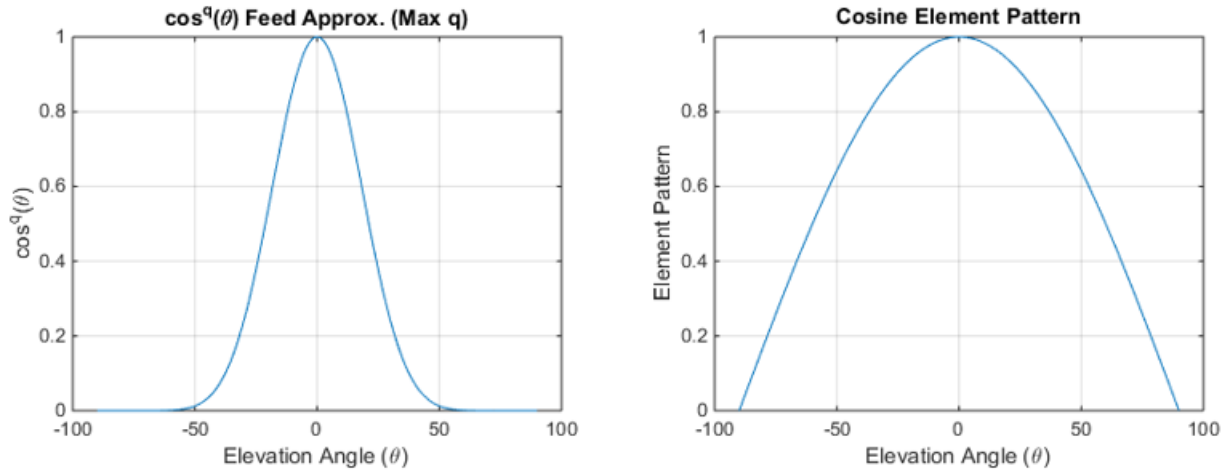

Fig. 24 – (a) Feed Pattern Approximation (b) Element Pattern Approximation

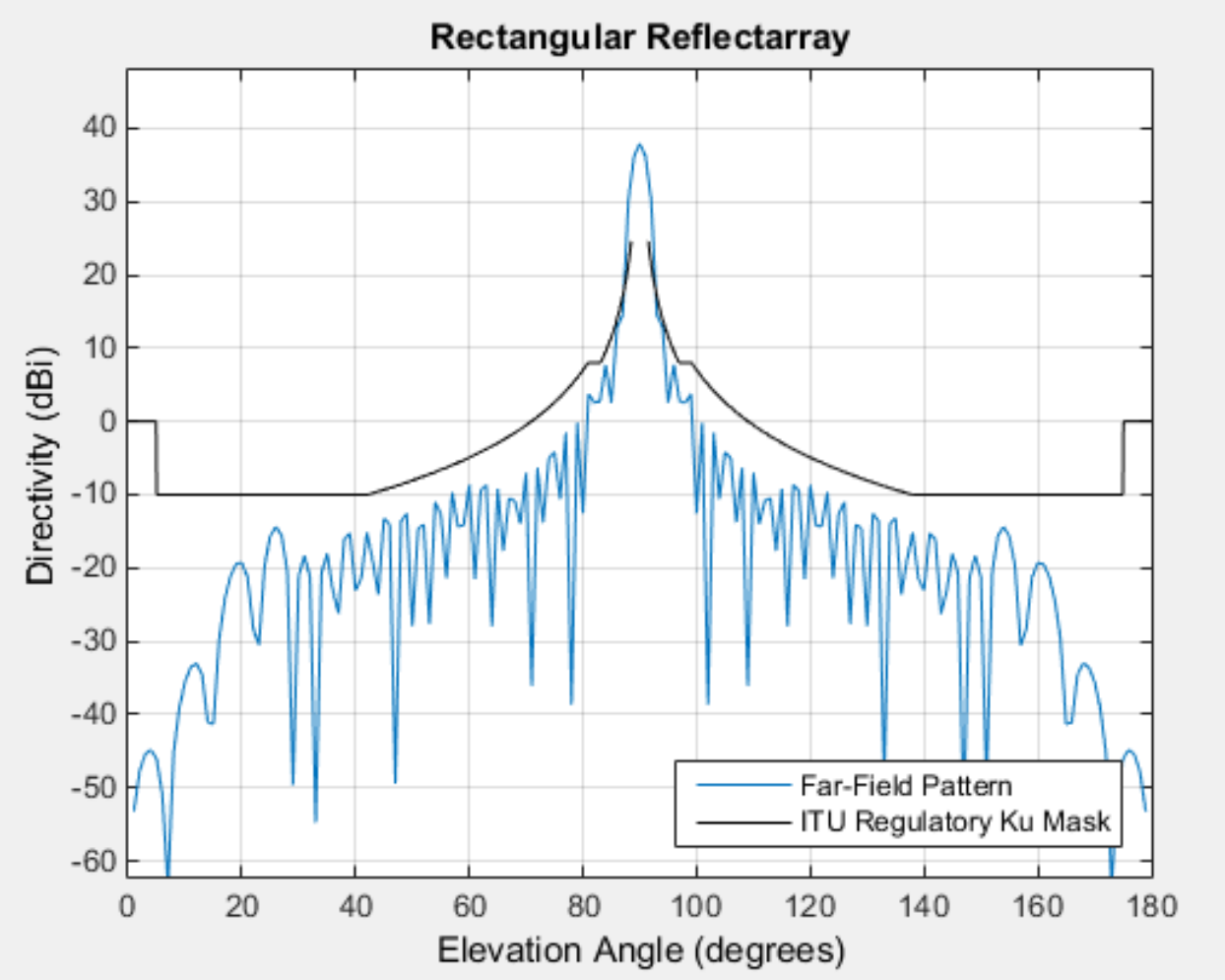

Fig. 25 – Far Field Approximation of the 25λ Reflectarray

Chapter 4

Design of Circular Reflectarray

In this section, a design process will be proposed for a circular element concentric-ring type reflectarray. This is a novel reflectarray design as circular FSS elements have only yet to be applied to AMCs not reflectarrays. Design examples will be given for both radial and circular polarizations corresponding to the polarizations for figures 8 (a) and (b) respectively at 12GHz with a diameter of ~25λ as in the Cartesian case. The geometries for these designs are given below in figures 26 (a) and (b) for radial and circular polarizations. These array geometries are chosen because for radial polarization we want longer and more numerous quasi-trapezoidal patch elements with short angular widths, while for circular polarization we want shorter and more densely packed quasi-trapezoidal patch elements with wide angular widths.

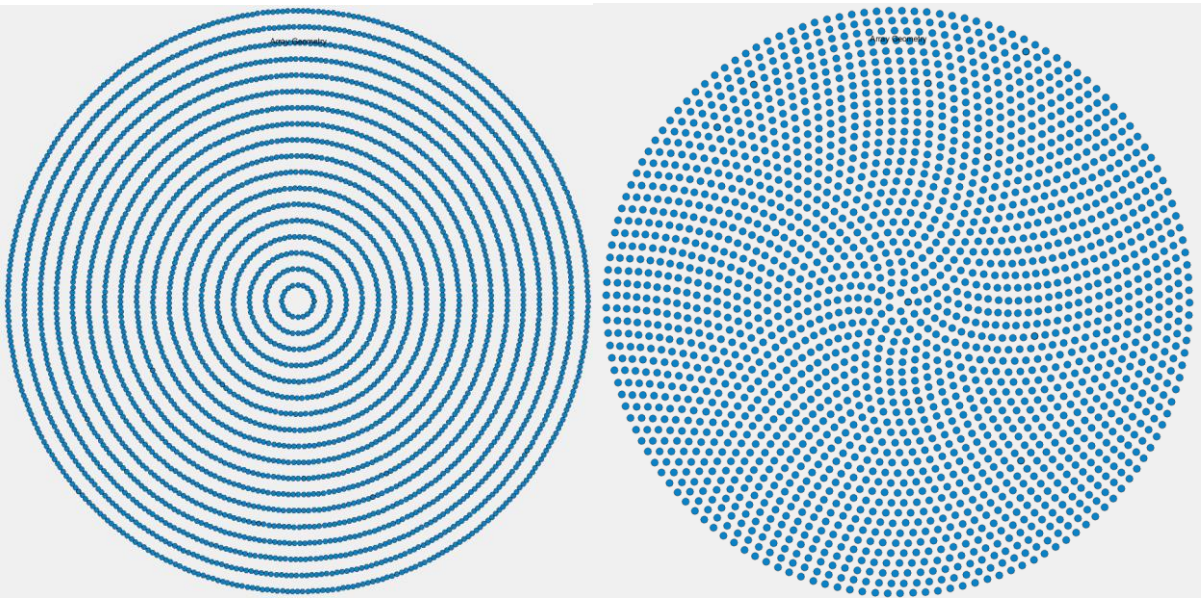

Fig. 26 – (a) Concentric-Ring Reflectarray #1
Radial Polarization (R=0.7λ, N=20i)
18 rows, 3,420 elements

(b) Concentric-Ring Reflectarray #2
Circular Polarization (R=0.43λ, N=5i)
29 rings, 2,175 elements

Each unit-ring is simulated separately from the others in HFSS in order to find the phase shift associated with that ring. For the radial polarization (figure 27), a PEC boundary condition is applied to the interior and exterior walls of the coax configuration to give the radial polarization in figure 8a. For the circular geometry (figure 28), a PMC boundary condition is applied to the interior and exterior walls of the coax configuration to give the circular polarization in figure 8b.

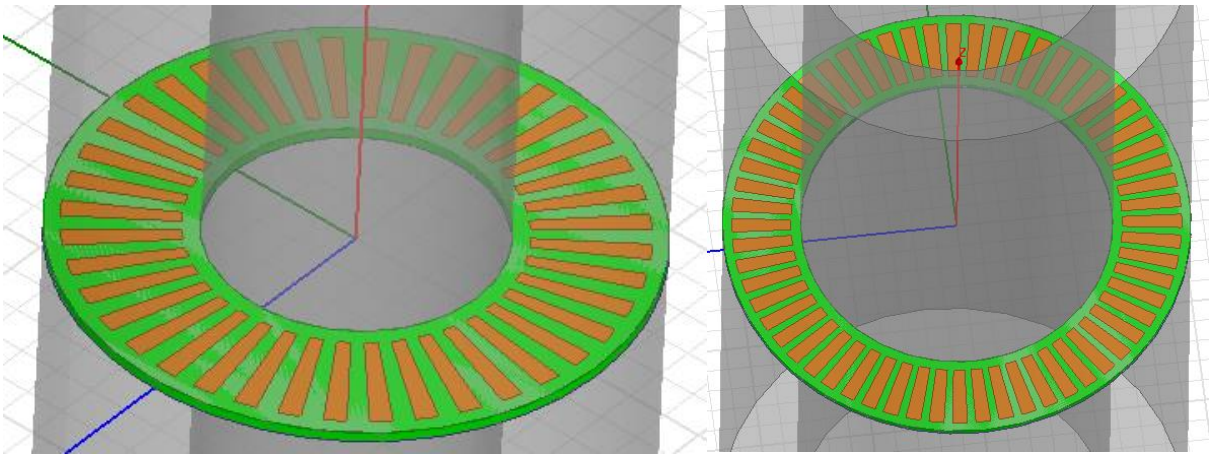

Fig. 27 – Rings #2 & #3 for the Radial Polarized Design

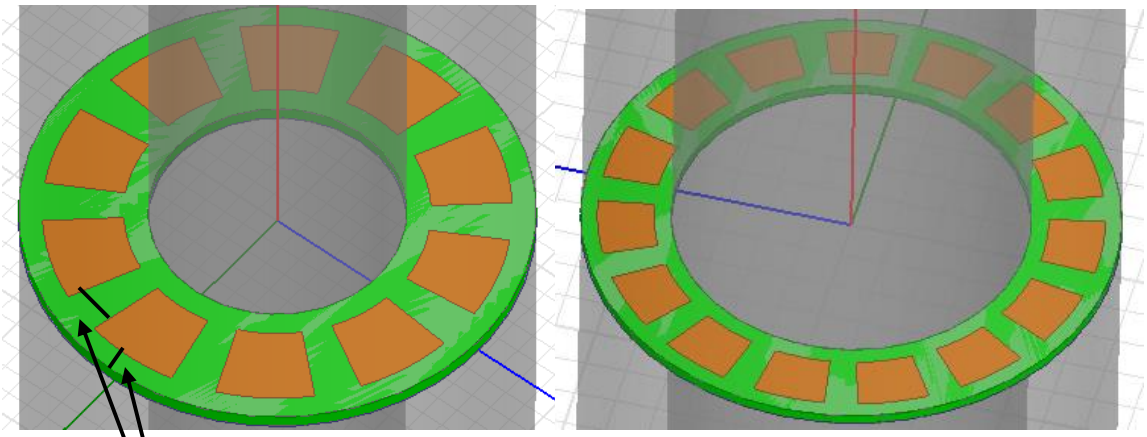

Fig. 28 – Rings #2 & #3 for the Circularly Polarized Design

Design Parameters: Angular Gap & Radial Gap

Radial Design Parameter Table	Radial Gap	Angular Gap Ratio (Ratio vs. Total Cell Size)	Angular Gap (Degrees)	Bandwidth	Resonant Frequency (GHz)
Ring #1	1.62	0.2399	4.32	4.25%	12
Ring #2	1.95	0.1168	1.05	3.42%	12
Ring #3	2.1	0.1470	0.88	3.42%	12
Ring #4	2.1	0.1470	0.66	3.42%	12

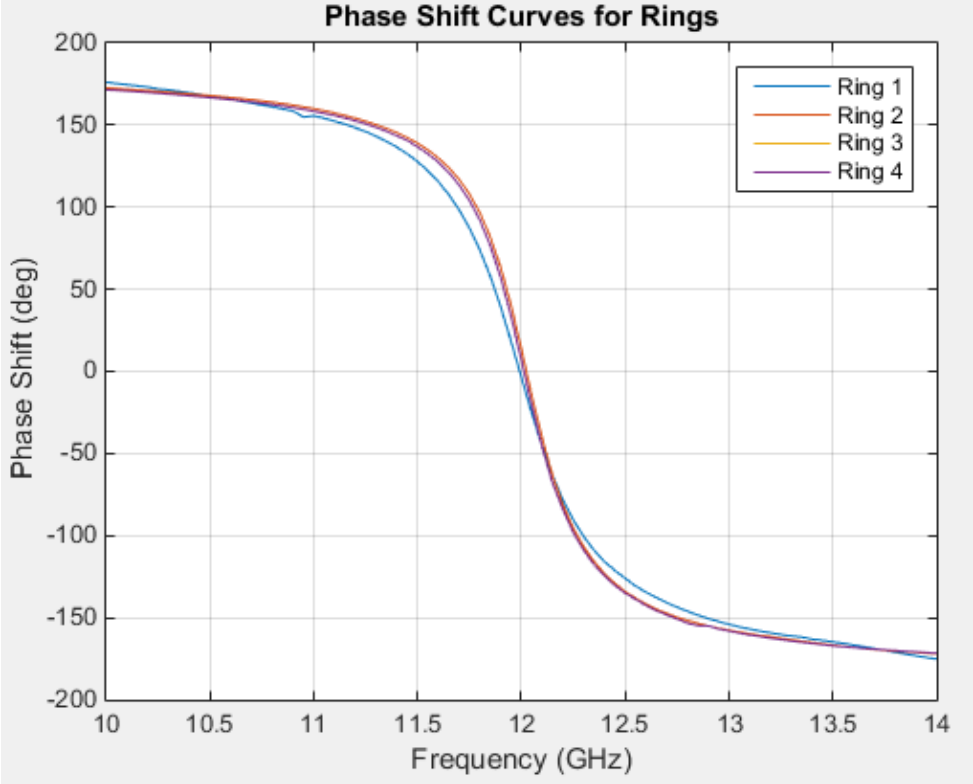

Fig. 29 – Radial Polarization Unit-Ring Phase Reflection Curves

The first design example explores the radial polarization unit-ring. As can be seen from the table, the design parameters must initially be changed for the first few rings, but after the 3rd ring, the design becomes stable and the parameters no longer need to vary.

Circular Design Parameter Table	Radial Gap (mm)	Angular Gap Ratio (Ratio vs. Total Cell Size)	Angular Gap (Degrees)	Bandwidth	Resonant Frequency (GHz)
Ring #2	2	0.3854	13.87	1.92%	12
Ring #3	2	0.3854	9.25	0.3%	11.72
Ring #4	2	0.3854	6.94	0.3%	10.72
Ring #5	2	0.3854	5.55	0.3%	10.47

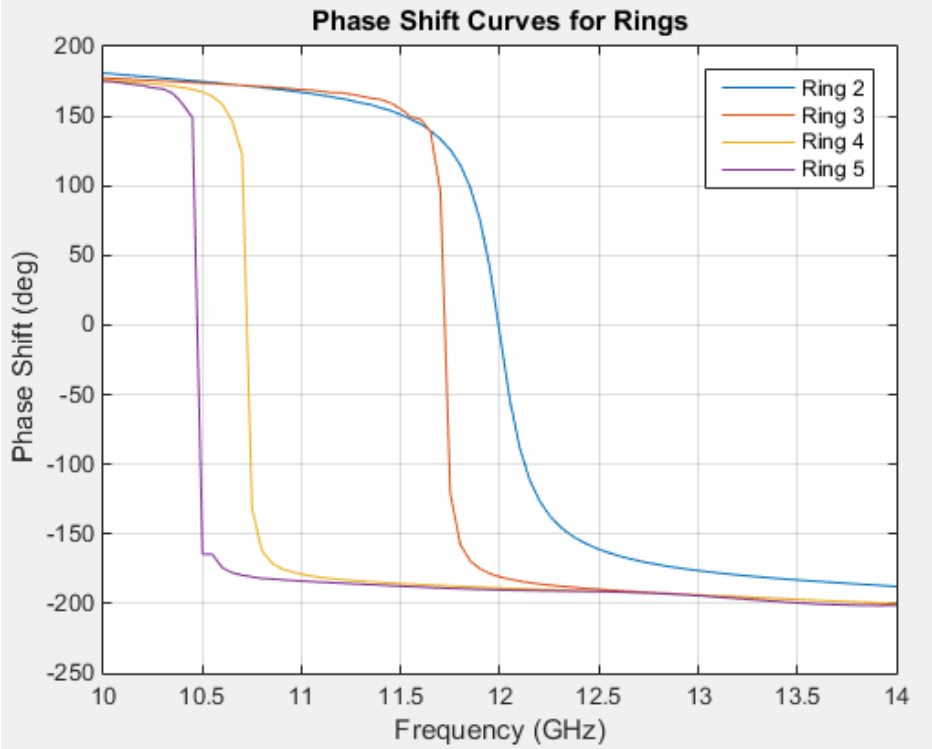

Fig. 30 – Circular Polarization Unit-Ring Phase Reflection Curves

To check and see if the circular polarization will follow the same design invariant principle, the second ring is optimized and then the parameters are held constant while the ring index increases. As can be seen in the table, the circular polarization case is much more sensitive to parameter variation, so more care must be taken when designing a reflectarray of this type.

Now that the array and phase characteristics have been found, the reflectarray far field pattern can be solved as in the rectangular case – but using a concentric-ring array topology. The concentric-ring array pattern has higher side lobe levels than the rectangular array. This fact is due to the use of the typical uniform pattern (i.e. r~fixed and Ni=N*i). Optimizing for Ni could yield lower side lobe levels by as much as 10dB (as in [39]), thus eliminating this issue. Figures 31 and 32 present the far field approximation for the designs. This field pattern is for a feed located with the center of the array for the patterns that follow (straight vertically up from the center of the arrays) with focal length to diameter (F/D) ratios of 1:1.

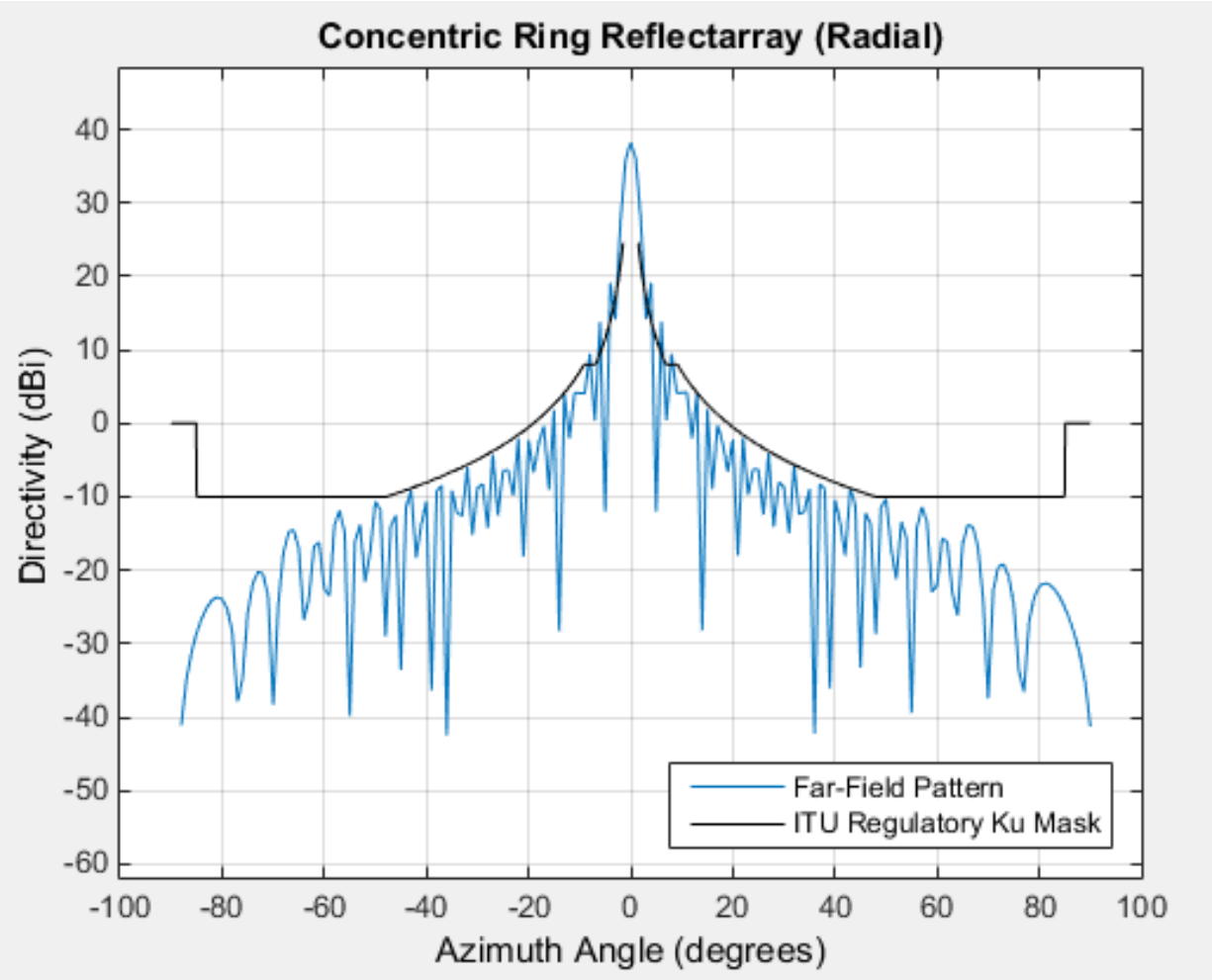

Fig. 31 – Far Field Approximation of the Concentric Ring Reflectarray (Radial Polarization)

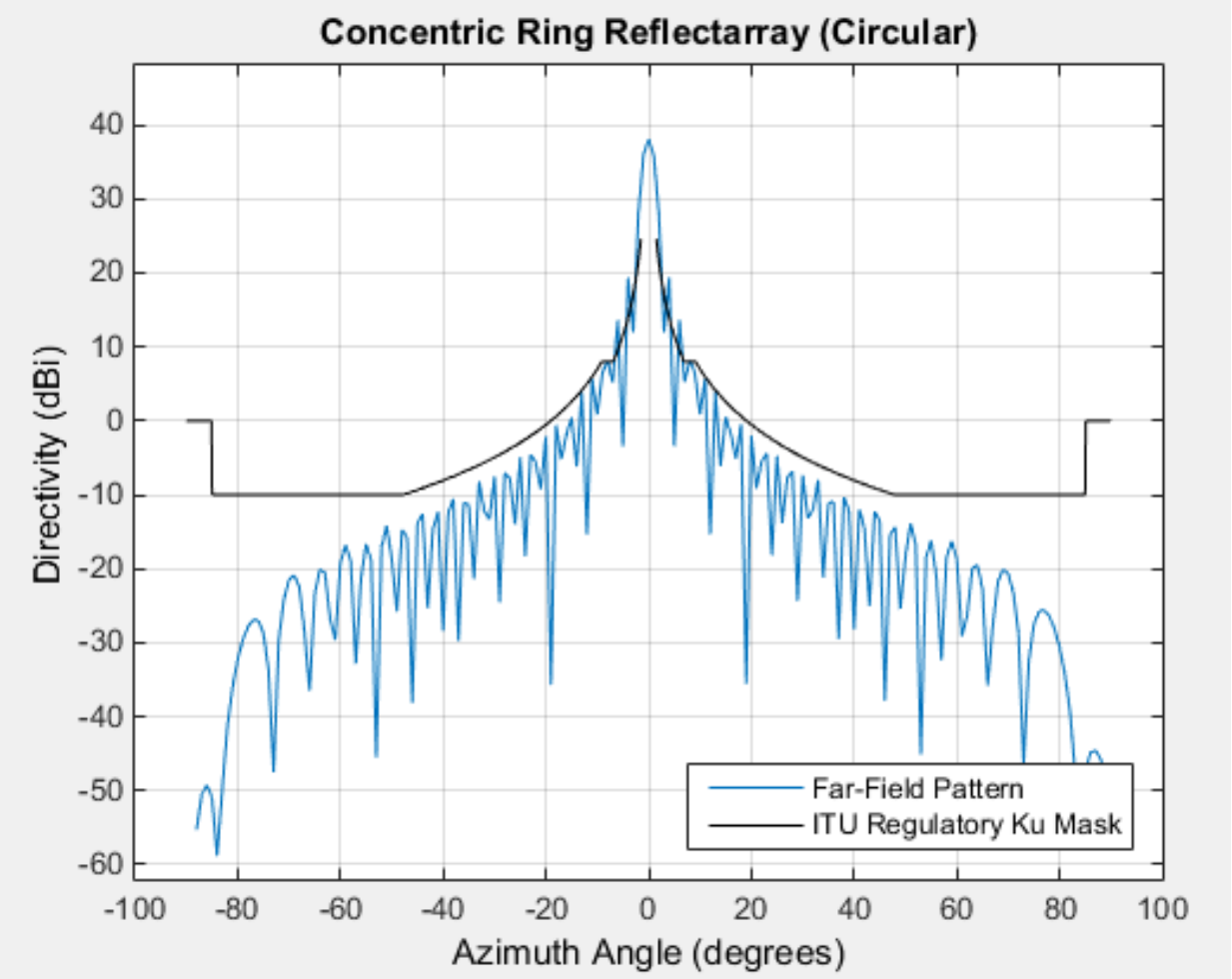

Fig. 32 – Far Field Approximation of the Concentric Ring Reflectarray (Circular Polarization)

Chapter 5

Conclusions

The table below compares the basic performance metrics of the three ~25λ reflectarrays.

Performance Comparison Table	Conventional (Horizontal Pol.)	Concentric Ring (Radial Polarization)	Concentric Ring (Circular Polarization)
Bandwidth (%)	1.2%	3.42%	1.92%
Directivity (dB)	37.91dB	38.19dB	38.06dB
Max Sidelobe Level (dB) (Relative to ITU Mask)	-1.96dB	+4.12dB	+5.30dB

It can be seen that: the conventional reflectarray has superior sidelobe characteristics, the concentric ring reflectarray geometries have superior bandwidths, and all designs have roughly the same directivities. After lowering sidelobe levels by the techniques discussed [39], the circular reflectarray could also have sidelobe margin. Thus, it is clear that a circular reflectarray can be designed with basic performance metrics (directivity, sidelobe level and bandwidth) that are comparable or even better than a conventional rectangular design.

REFERENCES

[1] L. Josefsson and P. Persson, Conformal array antenna theory and design. New York, NY, United States: Wiley-IEEE Press, 2006.

[2] A. F. Peterson, S. L. Ray, R. Mittra, Computational Methods for Electromagnetics. New York, NY: IEEE Press, 1998.

[3] J. Sarrazin, A. C. Lepage and X. Begaud, "Circular High-Impedance Surfaces Characterization," in *IEEE Antennas and Wireless Propagation Letters*, vol. 11, no., pp. 260-263, 2012.

[4] J. Huang and J. Encinar, Reflectarray Antennas. New York, NY, United States: Wiley-IEEE Press, 2008.

[5] C. A. Balanis, Antenna Theory: Analysis and Design, 3rd ed. New York, NY: John Wiley & Sons, 2005.

[6] W. L. Stutzman and G. A. Thiele, Antenna Theory and Design, 3rd ed. New York, NY: John Wiley & Sons, 2013.

[7] B. A. Munk, Frequency selective surfaces: Theory and design. New York, NY: John Wiley & Sons, 2000.

[8] Y. Rahmat-Samii and A. N. Tulintseff, "Diffraction analysis of frequency selective reflector antennas," in *IEEE Transactions on Antennas and Propagation*, vol. 41, no. 4, pp. 476-487, Apr 1993.

[9] F. O'Nians and J. Matson, "Antenna feed system utilizing polarization independent frequency selective intermediate reflector," U.S. Patent 3-231-892, Jan. 1966

[10] D. Sievenpiper, Lijun Zhang, R. F. J. Broas, N. G. Alexopolous and E. Yablonovitch, "High-impedance electromagnetic surfaces with a forbidden frequency band," in IEEE Transactions on Microwave Theory and Techniques, vol. 47, no. 11, pp. 2059-2074, Nov 1999.

[11] Fan Yang and Y. Rahmat-Samii, "Reflection phase characterizations of the EBG ground plane for low profile wire antenna applications," in IEEE Transactions on Antennas and Propagation, vol. 51, no. 10, pp. 2691-2703, Oct. 2003.

[12] J-M. Jin, The Finite Element Method in Electromagnetics, 3rd Ed. Hoboken, NJ: John Wiley & Sons, 2014.

[13] A. Taflove, S. C. Hagness, Computational Electrodynamics, The Finite Difference Time-Domain Method, 3rd Ed. Norwood, MA: Artech House, 2005.

[14] L. A. Costa, O. M. d. C. Pereira-Filho and F. J. S. Moreira, "Quasi-trapezoidal microstrip spherical patches and arrays," in *IET Microwaves, Antennas & Propagation*, vol. 10, no. 1, pp. 53-60, 1 9 2016.

[15] D. J. Gregoire, "3-D Conformal Metasurfaces," in IEEE Antennas and Wireless Propagation Letters, vol. 12, no. , pp. 233-236, 2013.

[16] C. Pelletti, G. Bianconi, R. Mittra and A. Monorchio, "Analysis of Finite Conformal Frequency Selective Surfaces via the Characteristic Basis Function Method and Spectral Rotation Approaches," in *IEEE Antennas and Wireless Propagation Letters*, vol. 12, no. , pp. 1404-1407, 2013.

[17] G. Tiberi, S. Bertini, A. Monorchio, G. Mazzarella and G. Montisci, "A Spectral Rotation Approach for the Efficient Calculation of the Mutual Coupling Between Rectangular Apertures," in *IEEE Antennas and Wireless Propagation Letters*, vol. 10, no. , pp. 131-134, 2011.

[18] A. C. Durgun, C. A. Balanis and C. R. Birtcher, "Reflection Phase Characterization of Curved High Impedance Surfaces," in IEEE Transactions on Antennas and Propagation, vol. 61, no. 12, pp. 6030-6038, Dec. 2013.

[19] M. A. Amiri, C. A. Balanis and C. R. Birtcher, "Analysis, Design, and Measurements of Circularly Symmetric High-Impedance Surfaces for Loop Antenna Applications," in *IEEE Transactions on Antennas and Propagation*, vol. 64, no. 2, pp. 618-629, Feb. 2016.

[20] D. Berry, R. Malech and W. Kennedy, "The reflectarray antenna," in *IEEE Transactions on Antennas and Propagation*, vol. 11, no. 6, pp. 645-651, Nov 1963.

[21] H. R. Phelan, "Spiralphase reflectarray for multitarget radar," Microwave Journal, Vol. 20, July 1977, pp. 67 – 73.

[22] C. S. Malagisi, "Microstrip disc element reflect array," Electronics and Aerospace Systems Convention, Sept. 1978, pp. 186 – 192.

[23] J. P. Montgomery, "A microstrip reflectarray antenna element," Antenna Applications Symposium, University of Illinois, Sept. 1978.

[24] R. E. Munson and H. Haddad, "Microstrip reflectarray for satellite communication and RCS enhancement and reduction," U.S. patent 4,684,952, Washington, D.C., August 1987.

[25] J. Huang, "Microstrip reflectarray," IEEE AP-S/URSI symposium, London, Canada, June 1991, pp. 612 – 615.

[26] T. A. Metzler, "Design and analysis of a microstrip reflectarray," Ph.D. Dissertation, University of Massachusetts, September 1992.

[27] Y. Zhang, K. L. Wu, C. Wu, and J. Litva, "Microstrip reflectarray: full-wave analysis and design scheme," IEEE AP-S/URSI symposium, Ann Arbor, Michigan, June 1993, pp. 1386 – 1389.

[28] D. M. Pozar and T. A. Metzler, “Analysis of a reflectarray antenna using microstrip patches of variable size,” Electronics Letters, April 1993, pp. 657 – 658.

[29] R. D. Javor, X. D. Wu, and K. Chang, “Beam steering of a microstrip flat reflectarray antenna,” IEEE AP-S/URSI symposium, Seattle, Washington, June 1994, pp. 956 – 959.

[30] D. C. Chang and M. C. Huang, “Multiple polarization microstrip reflectarray antenna with high efficiency and low cross - polarization,” IEEE Trans. Antennas Propagat., Vol. 43, August 1995, pp. 829 – 834.

[31] J. Huang, “Bandwidth study of microstrip reflectarray and a novel phased reflectarray concept,” IEEE AP - S/URSI symposium, Newport Beach, California, June, 1995, pp. 582 – 585.

[32] J. A. Encinar, “Design of a dual - frequency reflectarray using microstrip stacked patches of variable size,” Electronic Letters, Vol. 32, No. 12, June 1996. pp. 1049 – 1050.

[33] D. F. Sievenpiper, J. H. Schaffner, H. J. Song, R. Y. Loo and G. Tangonan, "Two-dimensional beam steering using an electrically tunable impedance surface," in *IEEE Transactions on Antennas and Propagation*, vol. 51, no. 10, pp. 2713-2722, Oct. 2003.

[34] S. V. Hum, M. Okoniewski and R. J. Davies, "Modeling and Design of Electronically Tunable Reflectarrays," in *IEEE Transactions on Antennas and Propagation*, vol. 55, no. 8, pp. 2200-2210, Aug. 2007.

[35] S. Xu, Y. Rahmat-Samii and W. A. Imbriale, "Subreflectarrays for Reflector Surface Distortion Compensation," in IEEE Transactions on Antennas and Propagation, vol. 57, no. 2, pp. 364-372, Feb. 2009.

[36] D. M. Pozar, S. D. Targonski and H. D. Syrigos, "Design of millimeter wave microstrip reflectarrays," in *IEEE Transactions on Antennas and Propagation*, vol. 45, no. 2, pp. 287-296, Feb 1997.

[37] E. Carrasco, J. A. Encinar and M. Barba, "Bandwidth Improvement in Large Reflectarrays by Using True-Time Delay," in *IEEE Transactions on Antennas and Propagation*, vol. 56, no. 8, pp. 2496-2503, Aug. 2008.

[38] S. M. A. Momeni Hasan Abadi, K. Ghaemi and N. Behdad, "Ultra-Wideband, True-Time-Delay Reflectarray Antennas Using Ground-Plane-Backed, Miniaturized-Element Frequency Selective Surfaces," in *IEEE Transactions on Antennas and Propagation*, vol. 63, no. 2, pp. 534-542, Feb. 2015.

[39] R. L. Haupt, "Optimized Element Spacing for Low Sidelobe Concentric Ring Arrays," in IEEE Transactions on Antennas and Propagation, vol. 56, no. 1, pp. 266-268, Jan. 2008.